Chemistry–A European Journal
Research Article
doi.org/10.1002/chem.202403218
Chemistry Europe
European Chemical Societies Publishing
www.chemeurj.org

Hot Paper

Hirshfeld Atom Refinement (HAR) and Complementary Bonding Analysis of Lithium *m*-Terphenylhydridoborates Containing B–H···Li Linkages

Daniel Duvinage,[a] Lorraine A. Malaspina,[a, b] Stefan Mebs,[c] Simon Grabowsky,*[a, b] Emanuel Hupf,*[a] and Jens Beckmann*[a]

The synthesis and characterization of the lithium *m*-terphenylhydridoborates $[Li(2,6\text{-}Mes_2C_6H_3)BH_3]_2$ (**1**), $Li(2,6\text{-}Mes_2C_6H_3)_2BH_2$ (**2**) and $Li(OEt_2)(2,6\text{-}Mes_2C_6H_3)_2BH_2$ (**3**) are reported. Hirshfeld Atom Refinement (HAR) of the experimentally obtained molecular structures by single-crystal X-ray crystallography allowed the determination of the exact positions of the hydrogen atoms. The bond situations of the various B–H···Li linkages were investigated by a complementary bonding analysis using various methods including atoms in molecules (AIM), electron localizability indicator (ELI–D), non-covalent interaction (NCI) index and the compliance matrix.

Introduction

Alkali metal salts of the tetrahydridoborate ion, $[BH_4]^-$, and organic derivatives thereof, $[R_nBH_{4-n}]^-$ (R = alkyl, aryl; n = 1–3), are widely employed as effective reducing agents in organic synthesis.[1] More recently, they also received interest as hydrogen storage materials.[2] Their reactivity may be fine-tuned by the judicious choice of the organic substituents R and the solvation of alkali metal ions, an observation that prompted extensive structural investigations into this compound class. As early as 1974, the X-ray structure of $[Li(DME)_2][Mes_2B(\mu\text{-}H)_2]$ revealed that the cation and anion are associated by two B–H···Li interactions.[3] Since that time, it has become clear that there is a wealth of (solvated) lithium hydridoborates, $[BH_4]^-$,[4–9] organohydridoborates, $[RBH_3]^-$,[10–22] diorganohydridoborates, $[R_2BH_2]^-$,[10,17,23–28] and triorganohydridoborates, $[R_3BH]^-$,[12] possessing B–H···Li linkages in their solid-state structures, which, however, are poorly understood in detail. This is partly due to the fact that the positions of the hydrogen atoms were difficult to locate by single-crystal X-ray crystallography using independent atom model (IAM) refinements. Consequently, bond parameters involving the hydrogen positions were not discussed due to lack of accuracy and precision. Hirshfeld atom refinement (HAR) is a rather new method that uses ab-initio calculated atomic form factors based upon aspherical atom partitioning of quantum-mechanical molecular electron densities.[29,30] It allows the free refinement of all atomic positions and anisotropic displacement parameters (ADPs), even for hydrogen atoms. Structural parameters for hydrogen atoms bonded to light elements determined using HAR are as accurate and precise as those obtained by neutron diffraction.[30]

In this work, we report the synthesis and full characterisation of three discrete lithium *m*-terphenylhydridoborates, namely $[Li(2,6\text{-}Mes_2C_6H_3)BH_3]_2$ (**1**), $Li(2,6\text{-}Mes_2C_6H_3)_2BH_2$ (**2**), and $Li(OEt_2)(2,6\text{-}Mes_2C_6H_3)_2BH_2$ (**3**), possessing two-electron-three-centre (2e3c) B–H···Li bonds, which were precisely and accurately determined using HAR. The experimental results are supported by a theoretical complementary bonding analysis[31] including electron density-based methods, such as atoms in molecules (AIM),[32] the electron localizability indicator (ELI–D),[33] the non-covalent interaction (NCI) index[34] and the compliance matrix.[35]

Results and Discussion

Synthesis and Characterization

The reduction of the previously known *m*-terphenylboron fluorides $2,6\text{-}Mes_2C_6H_3BF_2$ (**I**) and $(2,6\text{-}Mes_2C_6H_3)_2BF$ (**II**)[36] with lithium aluminium hydride, $LiAlH_4$, provided the lithium *m*-terphenylhydridoborates $[Li(2,6\text{-}Mes_2C_6H_3)BH_3]_2$ (**1**) and $Li(2,6\text{-}Mes_2C_6H_3)_2BH_2$ (**2**) as colourless crystalline solids in yields of 76 and 96 %, respectively (Scheme 1). Upon addition of diethylether, Et_2O, to **2**, $Li(OEt_2)(2,6\text{-}Mes_2C_6H_3)_2BH_2$ (**3**) was produced as colourless crystals in quantitative yield (Scheme 1).

[a] D. Duvinage, L. A. Malaspina, S. Grabowsky, E. Hupf, J. Beckmann
Institut für Anorganische Chemie und Kristallographie, Universität Bremen, Leobener Straße 7, 28359 Bremen, Germany
E-mail: simon.grabowsky@unibe.ch
emanuel.hupf@uni-bremen.de
j.beckmann@uni-bremen.de
[b] L. A. Malaspina, S. Grabowsky
Departement für Chemie, Biochemie und Pharmazie, Universität Bern, Freiestrasse 3, 3012 Bern, Switzerland
[c] S. Mebs
Institut für Experimentalphysik, Freie Universität Berlin, Arnimallee 14, 14195 Berlin, Germany

Supporting information for this article is available on the WWW under https://doi.org/10.1002/chem.202403218

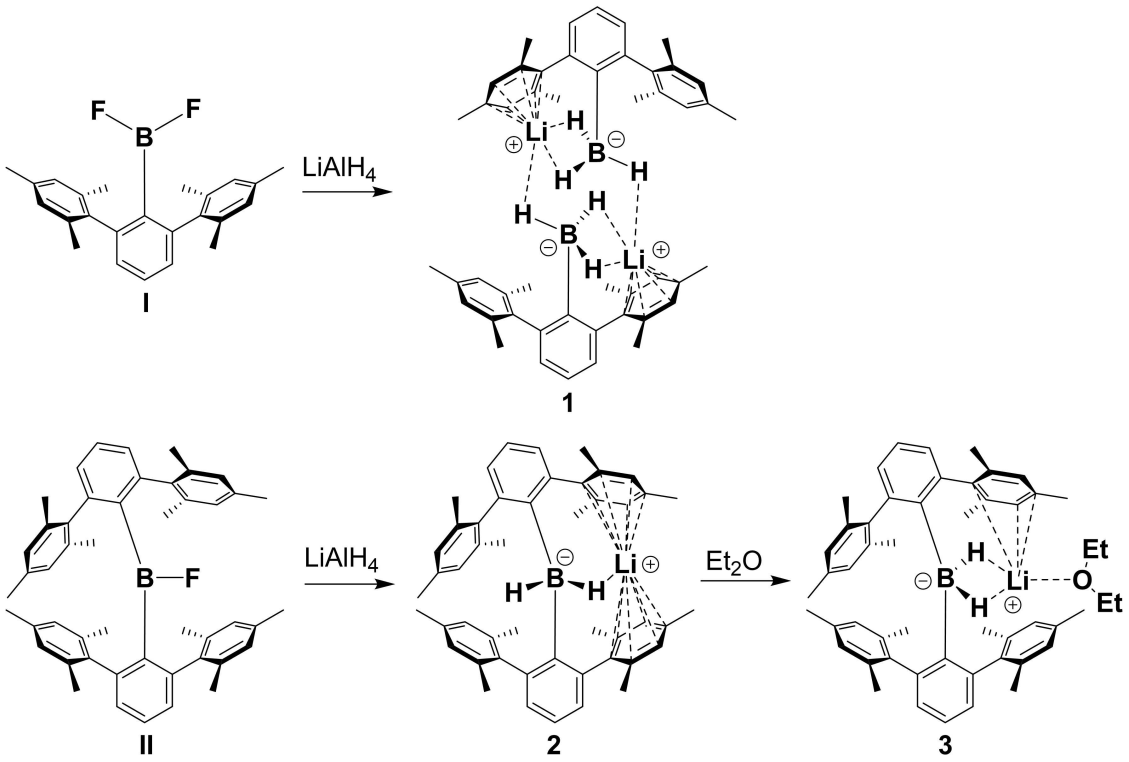

Scheme 1. Synthesis of lithium *m*-terphenylhydridoborates **1**–**3**.

In solution, **1**–**3** were characterized by multinuclear NMR spectroscopy (^{1}H, ^{7}Li, ^{11}B, and ^{13}C). The ^{11}B-NMR spectrum (C_6H_6) of **1** shows a quartet centered at $\delta = -30.9$ ppm with a coupling constant of $^{1}J(^{1}H\text{-}^{11}B) = 73$ Hz, which is consistent with values reported for other organotrihydridoborates.[10] The ^{1}H NMR spectrum (C_6H_6) of **1** reveals also a 1:1:1:1 quartet characteristic for the ^{11}B isotope centered at $\delta = -0.02$ ppm with a coupling constant of $^{1}J(^{1}H\text{-}^{11}B) = 71$ Hz. Unfortunately, the ^{7}Li NMR spectrum (C_6H_6) of **1** gave only a broad singlet at $\delta = -5.1$ ppm, which tentatively suggests a dynamic bond situation, presumably due to dissociation in solution. For the bis(*m*-terphenyl)boron species, the ^{11}B NMR spectra (C_6H_6) of **2** and **3** gave rise to triplets centred at $\delta = -14.5$ and -16.1 ppm, respectively, with coupling constants of $^{1}J(^{1}H\text{-}^{11}B) = 73$ and 72 Hz, which fall in the range of other diorganodihydridoborates.[10] In contrast to **1**, the ^{7}Li NMR spectra (C_6H_6) of **2** and **3** show sharp signals at $\delta = -2.5$ and -3.5 ppm, but no coupling information.

The molecular structures of **1**–**3** after HAR refinement of the crystal structures are displayed in Figures 1–3. In all three structures, the spatial arrangement of the B atoms is distorted tetrahedral. In **1**, the coordination sphere of the B atom is defined by a *CH*$_3$ donor set. The B1—H2 and the B1—H3 bond lengths of **1** are equal (1.206(7) Å) and identical within the experimental error compared to the HAR-refined (2,6-$Mes_2C_6H_3)_2$BH (1.203(4) Å) possessing a trigonal B atom.[36] The average terminal B–H bond length from 27 neutron-diffraction studies is 1.185(18) Å.[37] Hence, these two reference values indicate that B1—H2 and B1—H3 are not elongated (within the standard uncertainties) despite the interaction with the Li atom. The remaining B1—H1 bond length of **1** (1.222(7) Å) is slightly elongated. The computationally optimized dimeric geometry of **1** is more symmetric than the experimental solid-state structure and consequently the HAR-refined X-ray and neutron diffraction results (1.2190 Å, 1.2361 Å and 1.2364 Å) have a larger variance, which highlights the importance of reliable experimental determinations.

The IR-spectrum of **1** reveals three bands at $\tilde{\nu} = 2289$, 2170 and 2113 cm^{-1} in the expected area for B–H stretching vibrations. The computed values, derived from the frequency analysis, are at $\tilde{\nu} = 2342$, 2341, 2256, 2231 and 2194 cm^{-1}, respectively. However, close inspection of the vibrational modes reveal that these are not isolated B–H stretching vibrations, but strongly coupled with other vibrations.

In **1**, the Li atom engages in a η^6 coordination to one of the flanking mesityl groups (Li–C: 2.472(2)–2.555(2) Å) and is additionally coordinated to three H atoms with bond lengths of Li1···H1 2.134(7) Å, Li1···H2 2.099(7) Å and Li1a···H3 1.995(7) Å. In agreement with the observation that the B–H bonds are not significantly elongated because of the interaction with the Li atoms, there is no correlation between the experimentally determined B–H and Li···H bond lengths. As observed for the B–H bonds, the computed optimized Li–H bonds differ less from each other than the experimentally observed bonds with values of 1.9378, 1.9339 and 2.0209 Å, due to the difference in symmetry.

The structures of **2** and **3** are affected by the steric crowding induced by the two bulky *m*-terphenyl substituents. The

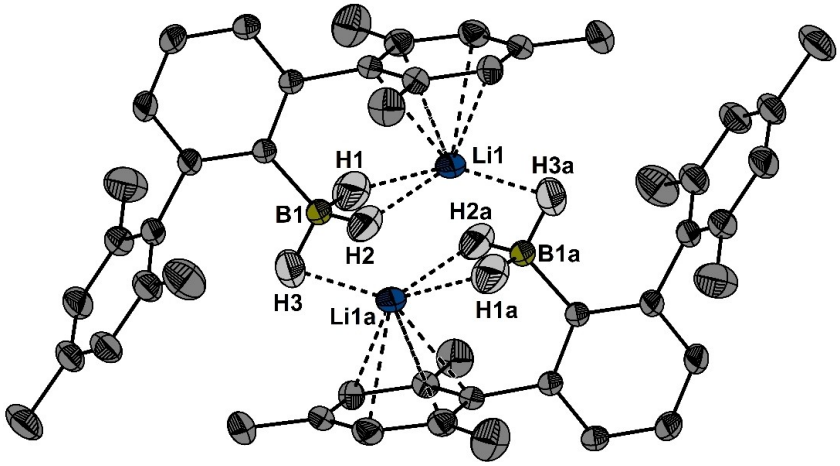

Figure 1. Molecular structure of **1** after HAR showing 50% probability of ADPs and the essential numbering scheme. Freely and anisotropically refined (B–)H atoms are shown, whereas all other H atoms are omitted for clarity, although also refined freely and anisotropically. Selected bond lengths [Å]: B1–H1 1.222(7), B1–H2 1.206(7), B1–H3 1.206(7), Li1···H1 2.134(7), Li1···H2 2.099(7), Li1a···H3 1.995(7).

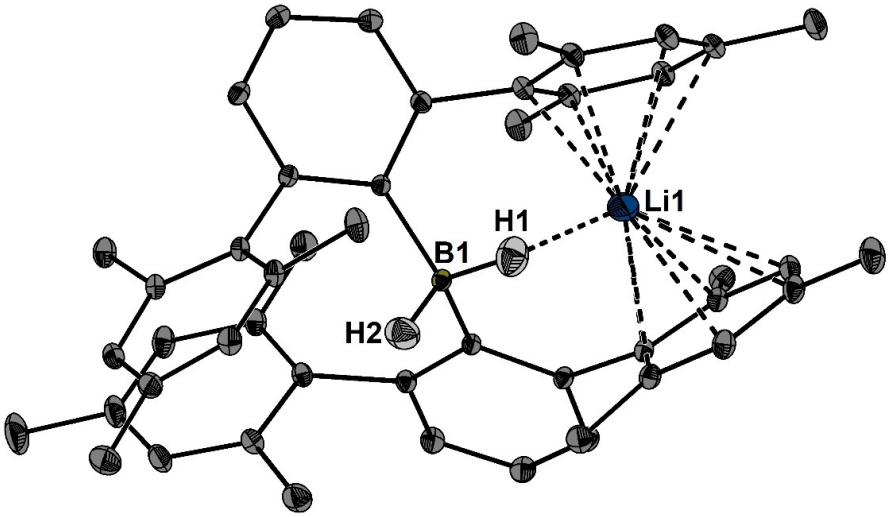

Figure 2. Molecular structure of **2** after HAR showing 50% probability of ADPs and the essential numbering scheme. Freely and anisotropically refined (B–)H atoms are shown, whereas all other H atoms are omitted for clarity, although also refined freely and anisotropically. Selected bond lengths [Å]: B1–H2 1.219(3), B1–H1 1.257(3), Li1···H1 1.817(3).

coordination spheres of the B atoms are defined by C_2H_2 donor sets. The C–B bond lengths of **2** (1.641(1) and 1.656(2) Å) and **3** (1.631(1) and 1.645(1) Å) are significantly longer than that of **1** (1.603(2) Å). The C–B–C angles of **2** (122.80(2)°) and **3** (117.52(4)°) are considerably larger than the tetrahedral angle. The B1–H2 bond length of **2** (1.219(3) Å) featuring an unperturbed terminal H atom is significantly shorter than the B1–H1 bond length of **2** (1.257(3) Å) and the B–H bond lengths of **3** (1.255(4) and 1.244(5) Å) being involved in B–H···Li linkages. These elongated B–H distances correlate with significantly shortened Li–H distances below 1.9 Å in **2** and **3** (further discussion in the next paragraph). Although the absolute values disagree, the trend is preserved in the computationally optimized geometries leading to B–H bond lengths of 1.2052 Å and 1.2424 Å for **2** as well as 1.2416 Å and 1.2381 Å for **3**, respectively. The IR-spectra of **2** and **3** each reveal bands at $\tilde{\nu}=$ 2223, 2166 and 2110 cm^{-1} and at $\tilde{\nu}=$2214, 2116 and 2081 cm^{-1}, respectively in the area of B–H stretching vibrations. Like in **1**, computed values are 2422 cm^{-1} and 2195 cm^{-1} for **2** as well as 2202 cm^{-1} and 2171 cm^{-1} for **3** show strong coupling with other vibrational modes and difference are most likely due to the higher symmetry.

In **2**, the Li atom engages in a η^6 coordination with two of the flanking mesityl groups (Li–C: 2.325(2)–3.030(1) Å), which resembles the coordination mode of the recently reported undistorted $[Li(\eta^6\text{-}C_6H_6)_2]^+$ cation having nearly co-planar benzene rings.[38] However, in **2**, the mesityl rings differ substantially from co-planarity due to the additional Li1···H1 interaction (1.817(3) Å, computed: 1.7071 Å), which is markedly shorter than those of **1**. In **3**, the Li atom coordinates only in a η^3-fashion (Li–C: 2.424(1)–2.938(1) Å) due to the coordination to the ether molecule, which accounts for a Li1–O1 bond of

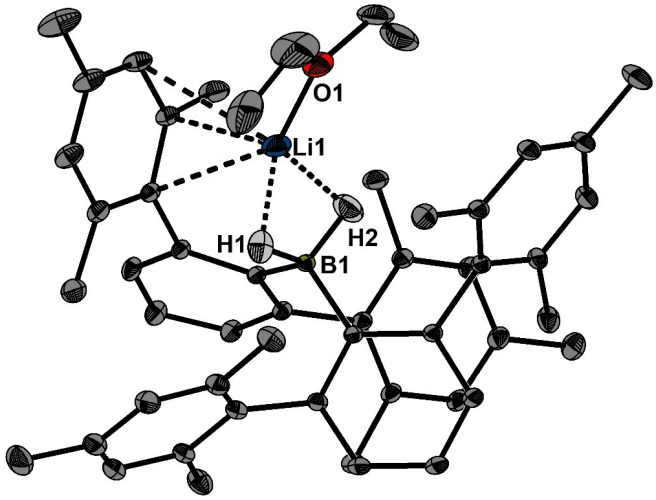

Figure 3. Molecular structure of **3** after HAR showing 50% probability of ADPs and the essential numbering scheme. Freely and anisotropically refined (B–)H atoms are shown, whereas all other H atoms are omitted for clarity, although also refined freely and anisotropically. Selected bond lengths [Å]: B1–H1 1.255(4), B1–H2 1.244(5), Li1–O1 1.888(1), Li1···H1 1.835(5), Li1···H1 1.893(4) Å.

1.888(1) Å. In addition, there are two Li···H interactions of 1.835(5) Å and 1.893(4) Å (computed 1.7607 and 1.8778 Å) about midway between those of **1** and **2**.

Computational Analysis

Density functional theory (DFT) computations were performed on **1**–**3** with the aim to analyze the B–H bonds and the Li···H interactions, as well as the hapticity of the lithium towards the mesityl units of the flanking terphenyl substituents by means of a complementary bonding analysis.[31] Selected topological and integrated bond properties are summarized in Table S2 of the Supporting Information. In all three investigated borates, a single Li···H bond critical point (bcp) is observed for each compound in a topological AIM analysis.[32] However, the bonding scenario is different in all three cases.

In **2**, the situation is most straightforward because one clear Li···H coordination is observed, whereas the second hydride points away from the lithium. This is manifested by the topological parameters found for the B–H bcps, which correlate with the significantly different B–H bond lengths discussed above. The non-coordinated B–H bond shows electron density values ($\rho(r)_{bcp}$) and Laplacians ($\nabla^2\rho(r)_{bcp}$) at the bcp of 1.14 e Å^{-3} and −4.3 e Å^{-5}, respectively. In comparison, the B–H···Li coordinated bond shows reduced electron density and a more positive Laplacian (0.95 e Å^{-3}/0.3 e Å^{-5}), which is indicative of a reduced strength of the covalent interaction in the latter one. This is further corroborated by a larger kinetic energy over electron density value ($G/\rho(r)_{bcp}$) in the coordinated Li···H interaction (Table S2). The electron density as well as the Laplacian at the Li···H bcp in **2** of 0.17 e Å^{-3} and 3.0 e Å^{-5}, respectively, compare well to respective values reported for Li···H interactions in $LiNMe_2BH_3$ (0.11 to 0.18 e Å^{-3} and 1.86 to 2.91 e Å^{-5}).[39] The Li···H interaction is dominated by ionic contributions as indicated by the strongly positive $G/\rho(r)_{bcp}$ value of 1.10 h e^{-1} with the total energy over electron density value ($H/\rho(r)_{bcp}$) being close to zero (0.12 h e^{-1}).

In **3**, both hydrides H1 and H2 point towards the lithium (compare Figure 3). Nevertheless, only a single Li···H bcp is found (Figure 4, left). The very large ellipticity of the Li···H bcp of 0.99 is an indication of an interaction also to the second hydride, despite the lack of a second bcp. Furthermore, the electron density minimum found along the direct Li···H axes are similar with values of 0.17 e Å^{-3} (0.18 e Å^{-3} at the bcp) and 0.14 e Å^{-3} (no bcp) as are the delocalization indices δ(Li|H) of 0.055 (with bcp) and 0.044 (no bcp). In an attempt to visualize the Li···H interaction, we plotted the electron density onto the Li AIM basin and it shows that the electron density is clearly distributed towards both hydrides (Figure 4, right). Hence, the B–H···Li interaction is best not described as two directed

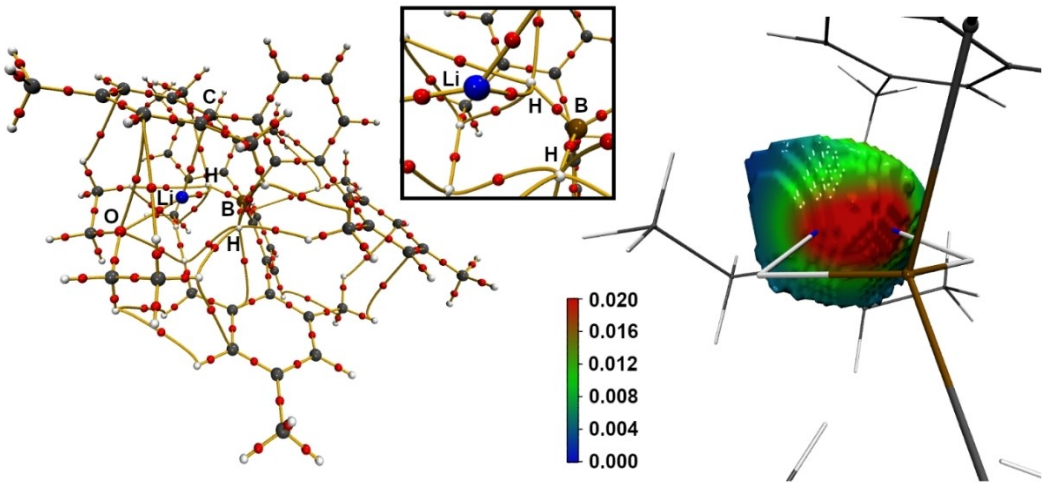

Figure 4. *left:* AIM molecular graph of **3** with bond critical points as red spheres with the inset providing an enlarged view on the Li···H region; *right:* electron density mapped on the Li AIM atomic basin (in units of e bohr^{-3}).

atom···atom interactions but as a BH_2···Li bifurcated linkage between molecular fragments.[40]

In **1**, the bridging Li atoms are situated between two BH_3 moieties. The AIM analysis reveals for each Li atom one Li···B and one Li···H bcp (Figure 5). Notably, these bcps are formed of opposing B-sides (Figure 5, inset). The electron densities (0.15 and 0.12 e Å^{-3}) and the Laplacians (2.8 and 2.1 e Å^{-5}) as well as the $G/\rho(r)_{bcp}$ (1.15 and 1.05 h e^{-1}) and $H/\rho(r)_{bcp}$ (0.13 and 0.14 h e^{-1}) values for both types of bcps are similar to the values of Li···H bcps found for **2** and **3** comprising predominantly ionic interaction (Table S2). However, the very large ellipticity of the Li···B bcp of 2.9 shows the extreme smearing of the electron density and indicates that the Li atoms are most likely interacting with two BH_2-moieties rather than interacting with one H- and one B-atom. This is further manifested upon inspection of the electron density distribution on the Li AIM basin which shows high smeared-out electron density values towards both H-atoms (Figure 5 right). Interestingly, the delocalization indices between the Li and those two H-atoms of δ(Li | H) of 0.035 and 0.038 are larger than the respective Li–B delocalization index of δ(Li | B) = 0.017 (Table S4), but yet very similar to the one, where a Li–H bcp is found (δ(Li | B) = 0.036). As for **2**, the interaction of the Li atom towards the H-atoms may be best described as a bifurcated H–Li–H_2 linkage in an electronically delocalized scenario between molecular fragments and not as directed atom···atom bonds.

The AIM atomic charges also point to the hydridic nature of the H-atoms being involved in interactions with the Li with charges varying between −0.64 e to −0.67 e in all three compounds (Table S3), which are slightly more negative compared to the H-atom (−0.57 e) of the non-coordinated B–H bond in **2**. The non-covalent interaction (NCI)[34] index of **1** and **3** is shown in Figure 6 (for **2**, see Figure S13).

The extended regions of non-covalency (green color) between the Li and BH_x moieties are indicative of predominantly dispersion interactions. However, there are disks of light blue color on the Li···H axes indicating that there are attractive forces between those atoms, but also that they are not directed but delocalized in space, in agreement with the conclusions from the AIM analyses above.

Within the ELI-D[33] topological analysis (Table S2), no disynaptic B–H bonding basins were found unlike we could assumed if the H atoms were fully hydridic, but instead only protonated monosynaptic B basins were observed. There are no

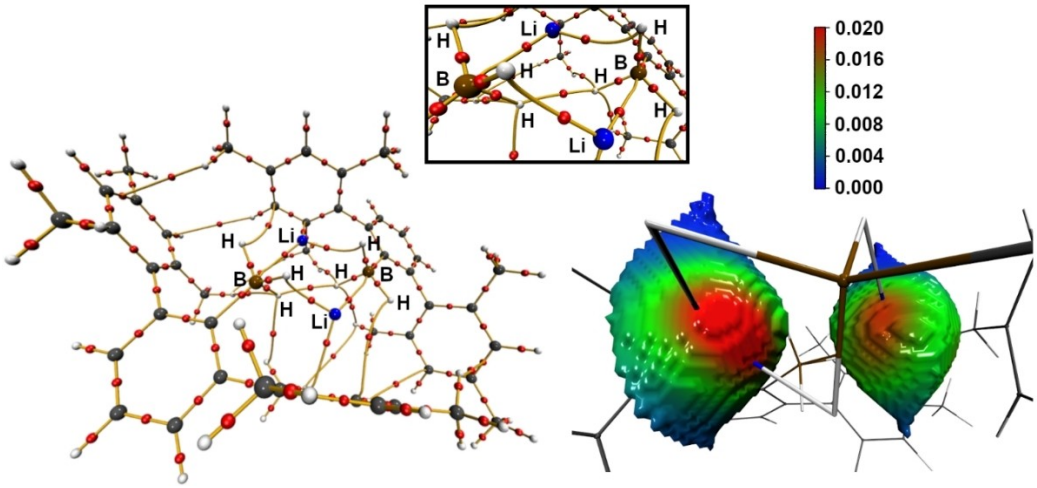

Figure 5. *left:* AIM molecular graph of **1** with bond critical points as red spheres with the inset providing an enlarged view on the central region; *right:* electron density mapped on the Li AIM atomic basins (in units of e bohr^{-3}).

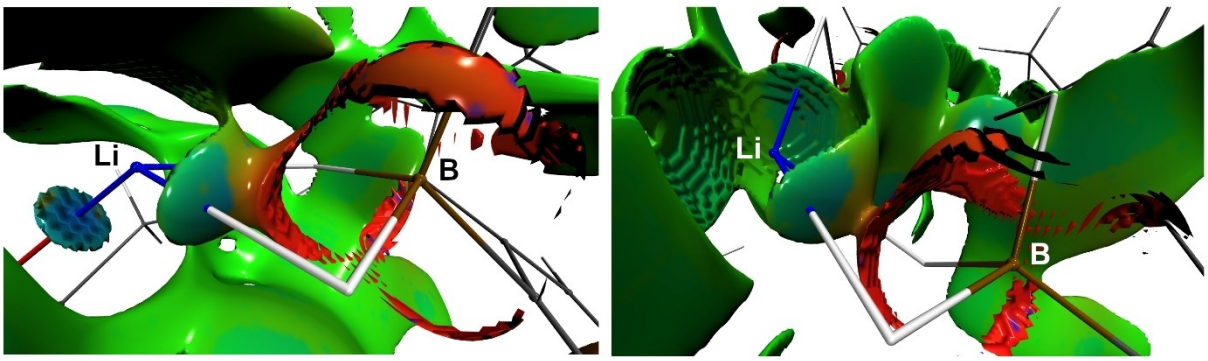

Figure 6. NCI *iso*-surfaces of **3** (left) and **1** (right) at s(r) = 0.6 color coded with sign(λ_2)ρ in a.u. Blue surfaces refer to attractive forces and red to repulsive forces. Green indicates weak interactions.

disynaptic Li–H bond basins either, in conjunction with predominantly ionic and dispersion interactions. The total number of electrons in the respective Li and H ELI core basins are very similar among the series of investigated borates and vary between 1.93–1.99 e for the H-atoms and 2.03 e for all Li-atoms.

The Li–H and B–H interactions were also investigated by the generalized compliance constants method.[35] Within this method, smaller numerical values indicate stronger interactions (Tables S5 and S6). The terminal, non-coordinative B–H bond in **2** gives rise to a constant C_{BH} of 0.300 Å mdyn^{-1}, which is smaller compared to the B–H bonds coordinated to Li in **2** (0.385 Å mdyn^{-1}) and **3** (0.365 Å mdyn^{-1} to 0.373 Å mdyn^{-1}). This correlates with the bond distances and the topological AIM parameters discussed above. The C_{LiB} and C_{LiH} values are significantly larger than the C_{BH} values, pointing to much weaker Li–H and B–Li interactions. In **2**, the C_{LiH} constant shows a smaller value (2.190 Å mdyn^{-1}) compared to C_{BLi} (5.682 Å mdyn^{-1}), whereas in **3**, this trend is reversed (C_{LiH} = 2.307 and 3.803 Å mdyn^{-1}; C_{LiB} = 1.690 Å mdyn^{-1}). However, in both compounds substantial coupling between the Li–H and B–Li fragments is observed of up to 1.847 Å mdyn^{-1} (**2**) and 1.493 Å mdyn^{-1} (**3**), which is significantly larger compared to the coupling between the respective Li–H and B–H fragments of 0.012 Å mdyn^{-1} (**2**) and −0.007/−0.048 Å mdyn^{-1} (**3**), which makes the interpretation difficult, but corroborates the picture of the delocalized fragment···fragment interaction found in AIM as well. In **1**, the C_{BH} values range from 0.321 to 0.369 Å mdyn^{-1} and are thus comparable to **3**; the C_{LiH} constants are larger than $C_{LiB,}$ but show also significant coupling of the fragments (Table S5). The Li-atoms in borates **1**, **2** and **3** are not solely coordinated by the BH_x units, but also by the flanking mesityl groups of the terphenyl ligands. The different Li–C_{mes} bond distances in the borates, *vide supra*, suggest that the coordination is not equally distributed which may lead to hapticities smaller than six. In each borate, only a single Li–C_{mes} bond path is detected in AIM. However, it is known that due to a rather flat electron density gradient in metallocene type compounds the AIM analysis fails to provide certain bcps and thus underestimates the hapticity, with better results being obtained by the inspection of the virial field.[41] Interestingly, in our case the virial field also yields only a single Li–C_{mes} bcp in all three borates.

In order to uncover the hapticity in the three borates **1**–**3**, we examined the delocalization indices of the Li–C_{mes} interactions and compared the results with the $[Li(\eta^6\text{-}C_6H_6)_2]^+$ cation[38] (optimized at the same level of theory), in which the delocalization indices are $\delta(Li|C_{mes}) = 0.023$ for all Li–C interactions (see Table S3).[41–46] In contrast, the delocalization indices for the borates **1**–**3** vary substantially. Each borate exhibits at least two larger $\delta(Li|C_{mes})$ values of 0.033 and 0.028 (**2**), 0.024 and 0.021 (**3**) as well as 0.024 and 0.019 (**1**). In **1** and **2**, one additional coordination with a medium $\delta(Li|C_{mes})$ value of 0.015 is observed, whereas all other values are between 0.001–0.009, which suggests a η^{2+x} coordination for borates **1** and **2** and a η^2 coordination for **3**. The different hapticities of the investigated borates in this study and the $[Li(C_6H_6)_2]^+$ can be visualized by mapping the electron density on the C_{mes} AIM basins (Figure 7). The $[Li(C_6H_6)_2]^+$ shows a perfectly ring-shaped distribution, whereas in borate **2** the electron density on the mesityl C AIM basins is not equally distributed and leads to regions with higher and lower electron densities on top of the six-membered ring.

Conclusions

The lithium *m*-terphenylhydridoborates $[Li(2,6\text{-}Mes_2C_6H_3)BH_3]_2$ (**1**), $Li(2,6\text{-}Mes_2C_6H_3)_2BH_2$ (**2**) and $Li(OEt_2)(2,6\text{-}Mes_2C_6H_3)_2BH_2$ (**3**) prepared in this study possess various B–H···Li linkages of different types. In **2**, there is a significant difference in B–H/Li···H distances from experiment and theory, AIM topological values of the electron density and values of the compliance constant between an unperturbed non-coordinated B–H bond and one in the B–H···Li linkage. This confirms that there is a measurable 3-center-2-electron interaction. In **1** and **3**, the complementary bonding analysis we performed led to the finding that there are no directed atom···atom interactions, but rather delocalized

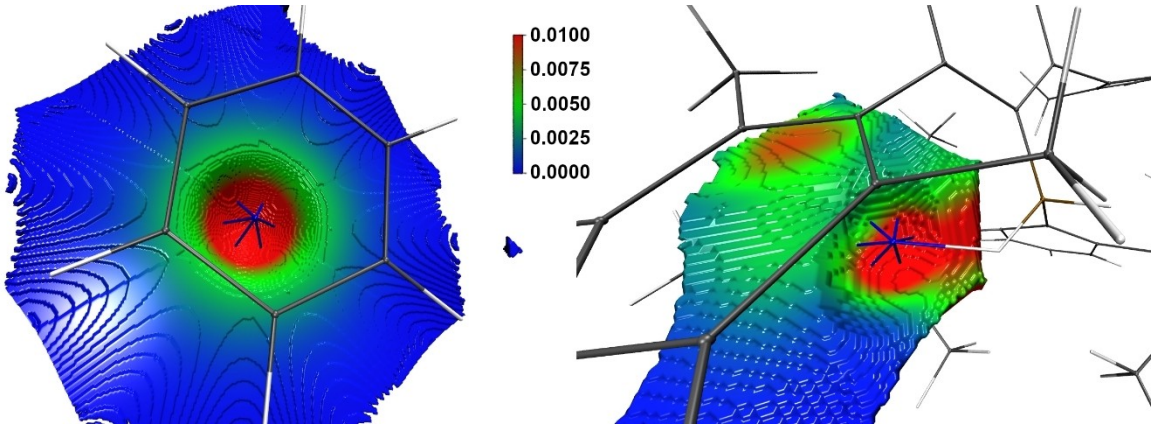

Figure 7. Electron density mapped on the C AIM atomic basins of the mesityl groups (in units of e bohr^{-3}) of $[Li(C_6H_6)_2]^+$ (left) and **2** (right). The Li atoms are in blue color and sit on top of the considered 6-membered ring. For a better visualization regarding the position of the mesityl unit, all six Li-C_{mes} sticks are included in the representation of borate **2** even if they are not bonds.

BH_2···Li (**3**) or H–Li–H_2 (**1**) bifurcated linkages. The forces underlying these interactions are ionic and dispersive, covering an extended region in space.

This study also shows that Hirshfeld Atom Refinement (HAR) of in-house X-ray data is a reliable source of accurate and precise hydrogen-atom positions and anisotropic displacement parameters. This makes much more cumbersome neutron-diffraction experiments obsolete for light-atom structures such as (lithium−)borates. Moreover, this study showed that DFT geometry optimization in the isolated state are more symmetric and therefore not representative of the experimentally obtained solid-state structures. Therefore, they did not yield reliable hydrogen-atom positions, rendering the HAR results even more important. Hence, this is the first study where B–H and Li···H distances were discussed and complementary bonding analyses were performed on alkali metal borates focusing on the impact of the hydrogen atoms.

Experimental Procedures

General Information

Unless otherwise stated, all reactions and manipulations were performed under inert atmosphere (argon) using anhydrous solvents. Reagents used in this work including $BF_3{\cdot}Et_2O$ and MeI were obtained commercially and were used as received. Commercial $LiAlH_4$ was purified by extraction with anhydrous Et_2O (thus removing insoluble gray material). The *m*-terphenylboron fluorides 2,6-$Mes_2C_6H_3BF_2$ (**I**) and (2,6-$Mes_2C_6H_3)_2BF$ (**II**) used as starting materials prepared following the published procedure.[36] Anhydrous dichloromethane, hexane, tetrahydrofurane and toluene were collected from an SPS800 mBraun solvent purification system and stored over 4 Å molecular sieves. Et_2O was dried by refluxing it over Na/benzophenone under argon atmosphere. Deuterated solvents were degassed and dried over 4 Å molecular sieves under argon.

Unless otherwise noted, NMR spectra were recorded at room temperature on a Bruker Avance 360 MHz and Avance 600 MHz spectrometer. ^{1}H, ^{13}C{^{1}H}, ^{11}B, ^{11}B{^{1}H} and ^{19}F NMR spectra are reported on the δ scale (ppm) and are referenced against $SiMe_4$, $BF_3{\cdot}Et_2O$ (15% in $CDCl_3$) and $CFCl_3$, respectively. ^{1}H and ^{13}C{^{1}H} chemical shifts are reported relative to the residual peak of the solvent ($CDHCl_2$ 5.32 ppm for CD_2Cl_2) in the ^{1}H NMR spectra, and to the peak of the deuterated solvent (CD_2Cl_2 53.84 ppm) in the ^{13}C{^{1}H} NMR spectra. The assignments of the ^{1}H and ^{13}C{^{1}H} resonance signals were made in accordance with the COSY, HSQC and HMBC spectra. The labelling schemes are attached to the ^{1}H and ^{13}C spectra.

The ESI HRMS spectra were measured on a Bruker Impact II spectrometer. Acetonitrile or dichloromethane/acetonitrile solutions ($c = 1{\cdot}10^{-5}$ mol L^{-1}) were injected directly into the spectrometer at a flow rate of 3 μL min^{-1}. Nitrogen was used both as a drying gas and for nebulization with flow rates of approximately 5 L min^{-1} and a pressure of 5 psi. Pressure in the mass analyser region was usually about $1{\cdot}10^{-5}$ mbar. Spectra were collected for 1 min and averaged. The nozzle-skimmer voltage was adjusted individually for each measurement. IR spectra were recorded on a *Nicolet* Thermo iS10 scientific spectrometer with a diamond ATR unit. The absorption bands are reported in cm^{-1} with indicated relative intensities: s (strong, 0–33% T); m (medium, 34–66% T), w (weak, 67–100% T), and br (broad).

Synthesis and Characterization of Li[2,6-$Mes_2C_6H_3BH_3$] (1)

$Mes_2C_6H_3BF_2$ (362 mg, 1.00 mmol, 1.00 eq.) and $LiAlH_4$ (80.0 mg, 2.00 mmol, 2.00 eq.) were placed in a Schlenk tube and cooled to −80 °C. To this mixture, diethylether (12 mL) was added. The reaction mixture was warmed up to 0 °C over the course of 3 h and then the solvent was removed under reduced pressure. The residual solid was dried at 60 °C/$5{\cdot}10^{-3}$ mbar. Afterwards, toluene (20 mL) was added and warmed up to 90 °C to extract the product. The suspension was filtered hot and the remaining solvent was removed under vacuum. The colourless solid was washed with *n*-hexane (3×5 mL) to afford the title compound as colourless solid (253 mg, 76%).

^{1}H NMR (600 MHz, C_6D_6):

$\delta = 7.22$ (t, $^3J(^1H\text{-}^1H) = 7.46$ Hz, 1H, H4), 6.92 (d, $^3J(^1H\text{-}^1H) = 7.46$ Hz, 2H, H3 and H5), 6.78 (s, 4H, H9 and H11), 2.09 (s, 6H, H14), 2.02 (s, 12H, H13 and H15), −0.02 (q, $^1J(^1H\text{-}^{11}B) = 70.90$ Hz, 3H, H16) ppm. ^{13}C{^{1}H} NMR (151 MHz, C_6D_6): $\delta = 146.0$ (s, C2 and C6), 144.1 (s, C7), 136.6 (s, C8 and C12), 136.6 (s, C10), 128.4 (s, C9 and C11), 126.5 (s, C3 and C5), 123. 7 (s, C4), 21.0 (s, C14), 20.7 (s, C13 and C15). ppm. ^{7}Li NMR (233 MHz, C_6D_6): $\delta = -5.1$ (s) ppm ^{11}B NMR (193 MHz, C_6D_6): $\delta = -30.9$ (q, $^1J(^{11}B\text{-}^1H) = 73.1$ Hz) ppm. HRMS ESI (m/z): $[M]^-$ calculated. for $C_{24}H_{25}BH_3$, 327.22895; found, 327.22889. IR (ATR, neat): $\tilde{\nu}$(B–H) = 2289 (m), 2170 (m), 2113 (m) cm^{-1}.

Synthesis and Characterization of Li[(2,6-$Mes_2C_6H_3)_2BH_2$] (2)

$(Mes_2C_6H_3)_2BF$ (656 mg, 1.00 mmol, 1.00 eq.) and $LiAlH_4$ (80.0 mg, 2.00 mmol, 2.00 eq.) were placed in a Schlenk tube, which was cooled with an ice bath. Diethylether (12 mL) was added slowly. The reaction mixture was stirred for 48 h. After this, the solvent was removed under reduced pressure and the residue was dried at 60 °C/$5{\cdot}10^{-3}$ mbar. The remaining solid was suspended in a mixture of toluene (10 mL) and *n*-hexane (20 mL) and warmed up to 80 °C. The suspension was filtered hot and the solvent was removed under reduced pressure. The remaining solid was washed with 2–5 mL *n*-hexane and dried at 80 °C/5 10^{-3} mbar to yield the title compound as a colourless solid (620 mg, 96%).

^{1}H NMR (600 MHz, C_6D_6):

$\delta = 7.00$ (t, $^3J(^1H\text{-}^1H) = 7.48$ Hz, 1H, H4), 6.79 (d, $^3J(^1H\text{-}^1H) = 7.48$ Hz, 2H, H3 and H5), 6.66 (s, 4H, H9 and H11), 2.15 (s, 6H, H14), 1.97 (s, 12H, H13 and H15), 1.67 (q, $^1J(^1H\text{-}^{11}B) = 69.75$ Hz, 1H, H16) ppm. ^{13}C{^{1}H} NMR (151 MHz, C_6D_6): $\delta = 152.0$ (q, $^1J(^{13}C\text{-}^{11}B) = 58.91$ Hz, C1) 145.7 (s, C2 and C6), 145.5 (s, C7), 137.1 (s, C8 and C12), 135.5 (s, C10), 129.4 (s, C3 and C5), 128.6 (s, C9 and C11), 123.7 (s, C4), 21.9 (s, C13 and C15), 21.1 (s, C14). ppm. ^{7}Li NMR (233 MHz, C_6D_6): $\delta = -2.51$ (s) ppm. ^{11}B NMR (193 MHz, C_6D_6): $\delta = -14.5$ (t, $^1J(^{11}B\text{-}^1H) = 69.8$ Hz) ppm. HRMS ESI (m/z): $[M]^-$ calculated. for $C_{48}H_{50}BH_2$, 639.41676; found, 639.41731. IR (ATR, neat): $\tilde{\nu}$(B–H) = 2223 (w), 2166 (m), 2110 (m) cm^{-1}.

Synthesis and Characterization of [Li(OEt_2)][(2,6-$Mes_2C_6H_3)_2BH_2$] (3)

Li[2,6-$Mes_2C_6H_3)_2BH_2$] (**2**) (65.6 mg, 0.1 mmol, 1.00 eq.) was dissolved in diethylether (4 mL). The solvent was removed under reduced pressure at room temperature to obtain [Li(OEt_2)][2,6-$Mes_2C_6H_3)_2BH_2$] as a colourless crystalline solid (73.0 mg, quant.).

^{1}H NMR (600 MHz, C_6D_6):

$\delta = 7.07$ (t, $^3J(^1H\text{-}^1H) = 7.46$ Hz, 1H, H4), 6.79 (d, $^3J(^1H\text{-}^1H) = 7.46$ Hz, 2H, H3 and H5), 6.72 (s, 4H, H9 and H11), 2.90 (q, $^3J(^1H\text{-}^1H) = 7.06$ Hz, 2H, CH_2 (OEt_2),) 2.21 (s, 6H, H14), 1.88 (s, 12H, H13 and H15), 1.76 (q, $^1J(^1H\text{-}^{11}B) = 71.6$ Hz), 0.78 (t, $^3J(^1H\text{-}^1H) = 7.06$ Hz, 3H, CH_3 (OEt_2)) ppm. $^{13}C\{^1H\}$ NMR (151 MHz, C_6D_6): $\delta = 147.2$ (s, C2 and C6), 145.5 (s, C7), 137.3 (s, C8 and C12), 135.0 (s, C10), 129.1 (s, C3 and C5), 128.8 (s, C9 and C11), 124.1 (s, C4), 66.3 (s, CH_2 (OEt_2)), 22.3 (s, C13 and C15), 21.1 (s, C14), 14.3 (s, CH_3 (OEt_2)) ppm. ^{7}Li NMR (233 MHz, C_6D_6): $\delta = -3.5$ (s) ppm. ^{11}B NMR (193 MHz, C_6D_6): $\delta = -16.1$ (t, $^1J(^{11}B\text{-}^1H) = 71.6$ Hz) ppm. HRMS ESI (m/z): $[M\text{-}Et_2O]^-$ calculated. for $C_{48}H_{50}BH_2$, 639.41676; found, 639.41731. IR (ATR, neat): $\tilde{\nu}$(B–H) = 2214 (w), 2116 (m), 2081 (m) cm^{-1}.

X-Ray Crystallography

Single crystals of **1** and **2** were grown by recrystallization from toluene and toluene/n-hexane (1 : 1), respectively. Single crystals of **3** were obtained by dissolving a sample in a minimal amount of ether and then letting the same volume of n-hexane slowly diffuse into the ether layer. X-ray diffraction data were collected at 200 K for **1** and at 100 K for **2** and **3** using an open flow nitrogen stream on a Bruker Venture D8 diffractometer with a Photon 100 detector in shutterless mode using a microfocus source (Mo$K\alpha$ = 0.71073 Å). All structures were solved using the dual-space algorithm in ShelXT[47] and refined against structure factor magnitudes $|F|^2$ with the use of SHELXL[47] (Independent Atom Model - IAM) within the WinGX program package.[48] All non-hydrogen atoms were refined using anisotropic displacement parameters. Hydrogen atoms were located from the Fourier difference map and had their positions and isotropic displacement parameter refined freely.

The geometries obtained from the IAM provided the initial model used as input for the subsequent Hirshfeld Atom Refinement (HAR)[29,30] performed using the Gaussian-HAR method with the lamaGOET[49] interface for Tonto[50] at the B3LYP/def2-TZVP level of theory. A self-consistent field of point monopoles and point-dipoles based on Hirshfeld charges for each atom in an 8 Å radius around the central formula unit was used in the iterative quantum chemical calculation step in order to simulate the crystal environment influence over the theoretical electron densities. HAR was performed against structure factor magnitudes F using a merged set of reflections, whereby negative $|F|^2$ reflections, reflections with $|F| < 3.0$ sigma($|F|$) (and 4.0 for **3**) and all systematic absences were pruned. All H atoms were refined freely and anisotropically within HAR. Refinement statistics for the HAR models can be seen in Table S1. Crystallographic data including structure factors for the structural analyses have been deposited with the Cambridge Crystallographic Data Centre, CCDC nos. 2346916–2346918. They can be downloaded free of charge from https://www.ccdc.cam.ac.uk/structures/.

Computational Results

Geometry optimizations of the isolated-molecule structures were performed using density functional theory (DFT) with the B3PW91[51] functional and the cc-pVTZ basis-set.[52] Initial molecular geometries were taken from the experimentally obtained crystal structures and, in case of $[Li(C_6H_6)_2]^+$, from the literature.[36] Subsequent frequency analyses confirmed all obtained structures to be local minima on the potential energy surfaces. Dispersion effects were modeled using Grimme's GD3BJ parameters.[53] All computations were performed with the Gaussian16 software.[54] The wavefunction files were used for a topological analysis of the electron density according to the Atoms-In-Molecules partitioning scheme[32] using AIMAll,[55] whereas DGRID[56] was used to generate and analyze the Electron-Localizability-Indicator (ELI–D) related real-space bonding descriptors[33] applying a grid step size of 0.05 a.u. The NCI[34] grids were computed with NCIplot.[57] AIM, ELI–D and NCI figures were generated with VMD.[58] The electron density values along the Li–H_8 axes were obtained with Multiwfn_3.8.[59] The determination of the compliance constants and compliance coupling constants were carried out with the COMPLIANCE software (version 3.0.2)[60] using the respective Gaussian *.log file containing the frequency analysis.

Acknowledgements

Deutsche Forschungsgemeinschaft (DFT) is gratefully acknowledged for financial support (GR 4451/2-1 and BE 3716/7-1). Open Access funding enabled and organized by Projekt DEAL.

Conflict of Interests

The authors declare no conflict of interest.

Data Availability Statement

Figures of NMR spectra as well as crystal and refinement data are given in the supporting information. Crystallographic information files (CIF) have been deposited with the Cambridge Crystallographic Data Centre (see above). Additional results from quantum chemical calculations are given in the supporting information. The raw data that support the findings of this study are available from the corresponding authors upon reasonable request.

Keywords: Hirshfeld atom refinement · X-ray crystallography · Hydrogen · Boron · Lithium

[1] H. C. Brown, *Boranes in Organic Chemistry*, Cornell University Press, London (UK), **1972**.
[2] S.-I. Orimo, Y. Nakamori, J. R. Eliseo, A. Züttel, C. M. Jensen, *Chem. Rev.* **2007**, *107*, 4111–4132.
[3] J. Hooz, S. Akiyama, F. J. Cedar, M. J. Bennett, R. M. Tuggle, *J. Am. Chem. Soc.* **1974**, *96*, 274–276.
[4] D. R. Armstrong, W. Clegg, H. M. Colquhoun, J. A. Daniels, R. E. Mulvey, I. R. Stephenson, K. Wade, *J. Chem. Soc. Chem. Commun.* **1987**, 630–632.
[5] J. E. Espidel, R. K. Harris, K. Wade, *Mag. Res. Chem.* **1994**, *32*, 166–172.
[6] A. Heine, D. Stalke, *J. Organomet. Chem.* **1997**, *542*, 25–28.
[7] H.-H. Giese, H. Nöth, H. Schwenk, S. Thomas, *Eur. J. Inorg. Chem.* **1998**, 941–949.
[8] H.-H. Giese, T. Habereder, H. Nöth, W. Ponikwar, S. Thomas, M. Warchhold, *Inorg. Chem.* **1999**, *38*, 4188–4196.
[9] H.-H. Giese, T. Habereder, J. Knizek, H. Nöth, M. Warchhold, *Eur. J. Inorg. Chem.* **2001**, 1195–1205.
[10] J. Knizek, H. Nöth, *J. Organomet. Chem.* **2000**, *614*, 168–187.
[11] D. Franz, M. Bolte, H.-W. Lerner, M. Wagner, *Dalton Trans.* **2011**, *40*, 2433–2440.
[12] D. Franz, A. H. Ilkhechi, M. Bolte, H.-W. Lerner, M. Wagner, *Eur. J. Inorg. Chem.* **2011**, *35*, 5414–5421.
[13] A. Das, A. Hübner, M. Weber, M. Bolte, H.-W. Lerner, M. Wagner, *Chem. Commun.* **2011**, *47*, 11339–11341.
[14] Ö. Seven, Z.-W. Qu, H. Zhu, M. Bolte, H.-W. Lerner, M. C. Holthausen, M. Wagner, *Chem. Eur. J.* **2012**, *18*, 11284–11295.

[15] Ö. Seven, M. Bolte, H.-W. Lerner, M. Wagner, *Organometallics* **2014**, *33*, 1291–1299.
[16] J. M. Breunig, F. Lehmann, M. Bolte, H.-W. Lerner, M. Wagner, *Organometallics* **2014**, *33*, 3163–3172.
[17] K. Samigullin, M. Bolte, H.-W. Lerner, M. Wagner, *Organometallics* **2014**, *33*, 3564–3569.
[18] T. Murosaki, S. Kaneda, R. Maruhashi, K. Sadamori, Y. Shoji, K. Tamao, D. Hashizume, N. Hayakawa, T. Matsuo, *Organometallics* **2016**, *35*, 3397–3405.
[19] E. Rochette, N. Bouchard, J. L. Lavergne, C. F. Matta, F.-G. Fontaine, *Angew. Chem. Int. Ed.* **2016**, *55*, 12722–12726.
[20] T. Kaese, T. Trageser, H. Budy, M. Bolte, H.-W. Lerner, M. Wagner, *Chem. Sci.* **2018**, *9*, 3881–3891.
[21] A. John, S. Kirschner, M. K. Fengel, M. Bolte, H.-W. Lerner, M. Wagner, *Dalton Trans.* **2019**, *48*, 1871–1877.
[22] C. Lenczyk, D. K. Roy, J. Nitsch, K. Radacki, F. Rauch, R. D. Dewhurst, F. M. Bickelhaupt, T. B. Marder, H. Braunschweig, *Chem. Eur. J.* **2019**, *25*, 13566–13571.
[23] R. E. Douthwaite, *Polyhedron* **2000**, *19*, 1579–1583.
[24] R. J. Wehmschulte, A. A. Diaz, M. A. Khan, *Organometallics* **2003**, *22*, 83–92.
[25] E. Januszewski, A. Lorbach, R. Grewal, M. Bolte, J. W. Bats, H.-W. Lerner, M. Wagner, *Chem. Eur. J.* **2011**, *17*, 12696–12705.
[26] E. von Grotthuss, M. Diefenbach, M. Bolte, H.-W. Lerner, M. C. Holthausen, M. Wagner, *Angew. Chem. Int. Ed.* **2016**, *55*, 14067–14071.
[27] E. Rochette, M.-A. Courtemanche, F.-G. Fontaine, *Chem. Eur. J.* **2017**, *23*, 3567–3571.
[28] T. Kaese, H. Budy, M. Bolte, H.-W. Lerner, M. Wagner, *Angew. Chem. Int. Ed.* **2017**, *56*, 7546–7550.
[29] a) D. Jayatilaka, B. Dittrich, *Acta. Cryst.* **2008**, *A64*, 383–393; b) S. C. Capelli, H.-B. Bürgi, B. Dittrich, S. Grabowsky, D. Jayatilaka, *IUCrJ* **2014**, *1*, 361–379.
[30] a) M. Woińska, S. Grabowsky, P. M. Dominak, K. Woźniak, D. Jayatilaka, *Sci. Adv.* **2016**, *2*, e1600192; b) L. A. Malaspina, A. Genoni, D. Jayatilaka, M. J. Turner, K. Sugimoto, E. Nishibori, S. Grabowsky, *J. Appl. Cryst.* **2021**, *54*, 718–729.
[31] *Complementary Bonding Analysis* (editor S.Grabowsky), De Gruyter: Berlin, Boston, **2021**.
[32] R. W. F. Bader, *Atoms in Molecules. A Quantum Theory*, Cambridge University Press, Oxford U. K. **1991**.
[33] M. Kohout, *Int. J. Quantum Chem.* **2004**, *97*, 651–658.
[34] E. R. Johnson, S. Keinan, P. Mori-Sánchez, J. Contreras-García, A. J. Cohen, W. Yang, *J. Am. Chem. Soc.* **2010**, *132*, 6498–6506.
[35] a) J. Grunenberg, N. Goldberg, *J. Am. Chem. Soc.* **2000**, *122*, 6045–6047; b) G. von Frantzius, R. Streubel, K. Brandhorst, J. Grunenberg, *Organometallics* **2006**, *25*, 118–121; c) K. Brandhorst, J. Grunenberg, *J. Chem. Phys.* **2010**, *132*, 184101–184107.
[36] D. Duvinage, L. A. Malaspina, S. Grabowksy, S. Mebs, J. Beckmann, *Eur. J. Inorg. Chem.* **2022**, e202200482.
[37] F. H. Allen, I. J. Bruno, *Acta Cryst.* **2010**, *B66*, 380–386.
[38] X. Jie, J. Li, C. G. Daniliuc, A.-L. Wübker, M. R. Hansen, H. Eckert, C. Mück-Lichtenfeld, G. Kehr, G. Erker, *Angew. Chem. Int. Ed.* **2021**, *60*, 22879–22884.
[39] D. J. Wolstenholme, J. Flogeras, F. N. Che, A. Decken, G. S. McGrady, *J. Am. Chem. Soc.* **2013**, *135*, 2439–2442.
[40] J. D. Dunitz, *IUCrJ* **2015**, *2*, 157–158.
[41] U. Flierler, M. Burzler, D. Leusser, J. Henn, H. Ott, H. Braunschweig, D. Stalke, *Angew. Chem. Int. Ed.* **2008**, *47*, 4321–4325.
[42] L. J. Farrugia, C. Evans, D. Lentz, M. Roemer, *J. Am. Chem. Soc.* **2009**, *131*, 1251–1268.
[43] S. Mebs, M. A. Chilleck, S. Grabowsky, T. Braun, *Chem. Eur. J.* **2012**, *18*, 11647–11661.
[44] S. Mebs, M. A. Chilleck, *Chem. Phys. Lett.* **2014**, *591*, 1–4.
[45] S. Mebs, M. A. Chilleck, K. Meindl, C. B. Hübschle, *J. Phys. Chem. A* **2014**, *118*, 4351–4362.
[46] S. Mebs, *Chem. Phys. Lett.* **2016**, *651*, 172–177.
[47] G. M. Sheldrick, *Acta Crystallogr., Sect. C: Struct. Chem.* **2015**, *71*, 3–8.
[48] L. J. Farrugia, *J. Appl. Cryst.* **2012**, *45*, 849–854.
[49] L. A. Malaspina, A. Genoni, S. Grabowsky, *J. Appl. Cryst.* **2021**, *54*, 987–995.
[50] D. Jayatilaka, D. J. Grimwood, *International Conference on Computational Science*, Springer Berlin Heidelberg, Berlin, Heidelberg **2003**.
[51] a) A. D. Becke, *J. Chem. Phys.* **1993**, *98*, 5648–5652; b) J. P. Perdew, J. A. Chevary, S. H. Vosko, K. A. Jackson, M. R. Pederson, D. J. Singh, C. Fiolhais, *Phys. Rev. B* **1992**, *46*, 6671–6687.
[52] a) T. H. Dunning, *J. Chem. Phys.* **1989**, *90*, 1007–1023; b) D. E. Woon, T. H. Dunning, *J. Chem. Phys.* **1993**, *98*, 1358–1371.
[53] S. Grimme, S. Ehrlich, L. Goerigk, *J. Comp. Chem.* **2011**, *32*, 1456–1465
[54] Gaussian 16, Revision C.01, M. J. Frisch, G. W. Trucks, H. B. Schlegel, G. E. Scuseria, M. A. Robb, J. R. Cheeseman, G. Scalmani, V. Barone, G. A. Petersson, H. Nakatsuji, X. Li, M. Caricato, A. V. Marenich, J. Bloino, B. G. Janesko, R. Gomperts, B. Mennucci, H. P. Hratchian, J. V. Ortiz, A. F. Izmaylov, J. L. Sonnenberg, D. Williams-Young, F. Ding, F. Lipparini, F. Egidi, J. Goings, B. Peng, A. Petrone, T. Henderson, D. Ranasinghe, V. G. Zakrzewski, J. Gao, N. Rega, G. Zheng, W. Liang, M. Hada, M. Ehara, K. Toyota, R. Fukuda, J. Hasegawa, M. Ishida, T. Nakajima, Y. Honda, O. Kitao, H. Nakai, T. Vreven, K. Throssell, J. A. Montgomery,, Jr., J. E. Peralta, F. Ogliaro, M. J. Bearpark, J. J. Heyd, E. N. Brothers, K. N. Kudin, V. N. Staroverov, T. A. Keith, R. Kobayashi, J. Normand, K. Raghavachari, A. P. Rendell, J. C. Burant, S. S. Iyengar, J. Tomasi, M. Cossi, J. M. Millam, M. Klene, C. Adamo, R. Cammi, J. W. Ochterski, R. L. Martin, K. Morokuma, O. Farkas, J. B. Foresman, D. J. Fox, Gaussian Inc., Wallingford CT, **2019**.
[55] AIMAll (Version 15.09.27), Todd A. Keith, TK Gristmill Software, Overland Park KS, USA, **2015** (aim.tkgristmill.com).
[56] M. Kohout, DGrid, version 5.1, Dresden, **2019**.
[57] J. Contreras-García, E. Johnson, S. Keinan, R. Chaudret, J.-P. Piquemal, D. Beratan, W. Yang, *J. Chem. Theory Comput.* **2011**, *7*, 625–632.
[58] W. Humphrey, A. Dalke, K. Schulten, *J. Mol. Graph.* **1996**, *14*, 33–38.
[59] T. Lu, F. Chen, *J. Comput. Chem.* **2012**, *33*, 580–592.
[60] K. Brandhorst, Grunenberg, *Chem. Soc. Rev.* **2008**, *37*, 1558–1567.

Manuscript received: August 27, 2024
Accepted manuscript online: October 16, 2024
Version of record online: November 12, 2024